ELSEVIER

Journal of Power Sources 55 (1995) 33–39

JOURNAL OF POWER SOURCES

Modified flooded spherical agglomerate model for gas-diffusion electrodes in alkaline fuel cells

Muhammad A. Al-Saleh, Selahattin Gultekin *, Sleem-ur-Rahman, Abdullah Al-Zakri

Department of Chemical Engineering, King Fahd University of Petroleum and Minerals, Dhahran-31261, Saudi Arabia

Received 2 August 1994; accepted 7 November 1994

Abstract

The spherical-grain mathematical model is modified and tested against experimental data for single-layer, gas-diffusion electrodes of alkaline fuel cells. The model assumes that the electrode is made of spherical agglomerates of Raney metal and polytetrafluoroethylene (PTFE) that are flooded with electrolyte; the gas occupies the macropores of the electrode. In addition to previous analysis of the diffusion and reaction in the grains, the modified model includes the resistance of gas diffusion into the macropores and a thin electrolyte film surrounding the grain. The original model and the modified model are both compared with experimental polarization data for hydrogen oxidation on an Ni/PTFE electrode in alkaline electrolyte. The newly developed model predicts accurately the experimental data in all regions.

Keywords: Alkaline fuel cells; Gas-diffusion electrodes; Spherical agglomerates

1. Introduction

In the authors' laboratory, a dry method is used to produce porous gas-diffusion electrodes for fuel cells. These electrodes have only one layer, unlike most fuel-cell electrodes that have two layers, namely, a gas-diffusion and an active layer. Numerous attempts have been made to model fuel-cell electrodes mathematically in order to obtain theoretical polarization behaviour and, thus, to optimize their structure and composition. Conventional cylindrical models, if applied to the single-layered electrodes, will not show the limiting-current behaviour due to the absence of a gas-diffusion layer and, thus, to the absence of a gas-diffusion resistance [1]. A thorough review regarding mathematical models for electrode polarization has been given by Celiker et al. [2,3]. In these publications, a new model has been proposed. This is called 'the spherical-grain model' in which the electrode is considered to have a single layer. The model assumes (based on surface analysis) that Raney metal particles are dispersed in the electrode as spherical grain that are flooded with the electrolyte, while the macropores (i.e., the space between the grains) are occupied by the gas phase. The spherical-grain model predicts that the current density will be almost linear with the overpotential. The previous model has been compared with experimental data obtained by Al-Saleh et al. [4] for a Raney Ni/PTFE electrode. The model agrees with the experimental data only at low temperatures and low overpotentials. At higher overpotentials and temperatures, part of the experimental data deviates from the model and indicates the approach to a limiting current. This discrepancy can be explained on the basis of neglected external mass-transfer resistances. In this paper, the spherical-grain model is modified by incorporating the mass-transfer resistance in the macropores for gas diffusion and by assuming the existence of a thin film of electrolyte around the spherical grains.

2. Modified flooded spherical agglomerate model

The electrode is assumed to be made of porous, spherical, catalyst grains that are held together by fine PTFE strands. The space between these spheres constitutes the macroporosity. The presence of the PTFE strands renders these macropores hydrophobic. Therefore, no electrolyte remains in the macropores. The gas has first to diffuse into the macropores before it reaches the grain. In this modified model, the resistance associated with macropore diffusion has been included. Besides this, it is proposed that the hydrophilic grain is surrounded by a stagnant film of electrolyte of constant

* Corresponding author.

SSDI 0378-7753(94)02161-U

thickness. The reactant gas is dissolved at the outer surface, and then diffuses through the stagnant film to reach the surface of the flooded catalyst grain. Further diffusion of these molecules takes place inside the grain with simultaneous reaction. The ionic conductivity path (explained previously [3] in terms of narrow electrolyte bridges between the grains) is more convincing now since the electrolyte film is taken to surround the grain. The working mechanism and the structure of the electrode are shown schematically in Fig. 1. The resistances in the different sections of the diffusion path of the gas are also shown.

For the mathematical development of the modified model, it is necessary to make the following assumptions:

(i) Raney catalyst–PTFE grains are spherical, identical in size/structure activity, isopotential, distributed homogeneously in the electrode, flooded with electrolyte, and touching one another.

(ii) There exists a thin layer of the electrolyte on the surface of each agglomerate. This film helps in the ionic and electronic transport across the dissolved gas.

(iii) The local current density in the grain is given by the Butler–Volmer equation.

(iv) Diffusion of the dissolved gas in the grain and the film occurs in the radial direction only, while the macropores diffusion is in an axial direction only.

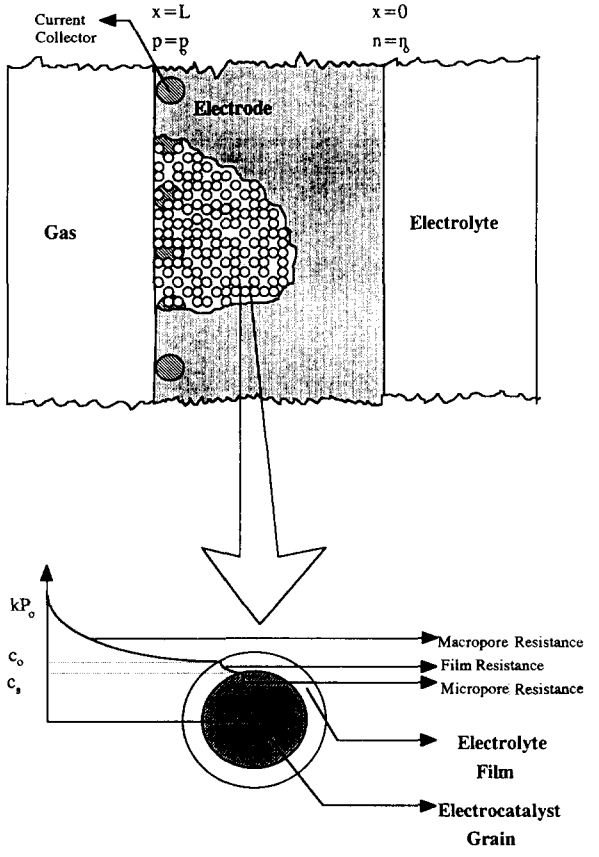

Fig. 1. Schematic diagram of fuel-cell electrode and Raney Ni/PTFE grain.

(v) The potential changes only across the thickness of the electrode.

(vi) There is no kinetic limitation on the dissolution of gas in the electrolyte.

(vii) The ionic concentration equilibration along the electrode is achieved by an evaporation/condensation mechanism.

The modified model is based on analysis of the grain, the film and the macropore. These analyses are then used with Ohm's law to describe the relationship between current density and overpotential.

2.1. The grain

In the grain, the dissolved gases are diffusing radially and reacting simultaneously. The local current density in a grain at plane x in the electrode is given by the Butler–Volmer equation:

$$i = i_0\left[\frac{C}{C_0}\exp\left(\frac{\alpha z F\eta(x)}{R_g T}\right) - \exp\left(\frac{-(1-\alpha)zF\eta(x)}{R_g T}\right)\right] \quad (1)$$

The rate of consumption of the reactant gas in the grain in terms of mol cm^{-3} s^{-1} is given by:

$$r_{gas} = \frac{ia}{nF} \quad (2)$$

The mass conservation equation with simultaneous diffusion and reaction under steady-state conditions is given by:

$$\frac{D_{le}}{r^2}\frac{\partial}{\partial r}\left[r^2\frac{\partial C(x,r)}{\partial r}\right] - r_{gas} = 0 \quad (3)$$

Combining Eqs. (1) to (3) with necessary rearrangements yields:

$$\frac{1}{r^2}\frac{\partial}{\partial r}\left[r^2\frac{\partial C(x,r)}{\partial r}\right] = A_1\left\{\frac{C(x,r)}{C_0}A_2 - A_3\right\} \quad (4)$$

where,

$$A_1 = \frac{i_0\alpha}{nFD_{le}} \quad (5)$$

$$A_2 = \exp\left[\frac{\alpha z F\eta(x)}{R_g T}\right] \quad (6)$$

$$A_3 = \exp\left[\frac{-(1-\alpha)zF\eta(x)}{R_g T}\right] \quad (7)$$

The boundary conditions are:

$$r = R \qquad C = C_s$$

$$r = 0 \qquad \frac{\partial C}{\partial r} = 0$$

The analytic solution of Eq. (4) is:

$$\frac{C(x,r)}{C_0} = \left[\frac{C_s}{C_0} - \frac{A_3}{A_2}\right]\frac{R\sinh(r\sqrt{A_1A_2/C_0})}{r\sinh(R\sqrt{A_1A_2/C_0})} + \frac{A_3}{A_2} \quad (8)$$

$$\left(\frac{dC(x,r)}{dr}\right)_{r=R} = C_0\left[\frac{C_s}{C_0} - \frac{A_3}{A_2}\right] \times\left[\sqrt{\frac{A_1A_2}{C_0}}\coth\left(R\sqrt{\frac{A_1A_2}{C_0}}\right) - \frac{1}{R}\right] \quad (9)$$

2.2. The film

With the presence of an electrolyte film around the spherical grains, the dissolved gas must diffuse first into the film surrounding the spherical grains. If the concentration at the outer surface of the film is $kp(x)$, while at the interface of film and grain, is C_S, then the continuity equation for the diffusing system at steady state is given by:

$$D_l\left[\frac{1}{r^2}\frac{\partial}{\partial r}\left(r^2\frac{\partial C_f}{\partial r}\right)\right] = 0 \quad (10)$$

with the boundary conditions:

$r=R$ $\quad C_f = C_s$

$r=R+\delta$ $\quad C_f = kp(x)$

The solution of Eq. (10) with these boundary conditions is:

$$\left(\frac{\partial C_f}{\partial r}\right)_{r=R+\delta} = \frac{R(kp(x)-C_s)}{\delta(R+\delta)} \quad (11)$$

At the interface between the film and the grain, the following mass balance holds:

$$4\pi(R+\delta)^2 D_l\left(\frac{\partial C_f}{\partial r}\right)_{r=R+\delta} = 4\pi R^2 D_{le}\left(\frac{\partial C}{\partial r}\right)_{r=R} \quad (12)$$

Substituting $\left(\frac{\partial C}{\partial r}\right)_{r=R}$ and $\left(\frac{\partial C_f}{\partial r}\right)_{r=R+\delta}$ from Eqs. (9) and (11) into Eq. (12) yields:

$$C_s = \frac{kp(x) + \frac{R\delta D_{le}C_0A_3}{(R+\delta)D_lA_2}\left[\sqrt{\frac{A_1A_2}{C_0}}\coth\left(R\sqrt{\frac{A_1A_2}{C_0}}\right) - \frac{1}{R}\right]}{1 + \frac{R\delta D_{le}}{(R+\delta)D_l}\left[\sqrt{\frac{A_1A_2}{C_0}}\coth\left(R\sqrt{\frac{A_1A_2}{C_0}}\right) - \frac{1}{R}\right]} \quad (13)$$

2.3. The macropores

In the hydrophobic macropores, the reactant gas is diffusing and is being consumed simultaneously under the following mass-conservation conditions:

$$D_g\frac{d^2p}{dx^2} - R^* = 0 \quad (14)$$

where D_g is the effective gas diffusivity in the macropores. The term R^* is the rate of consumption per unit volume of the electrode and is given by:

$$R^* = \left[4\pi R^2 D_{le}\left(\frac{\partial C}{\partial r}\right)_{r=R}\right]\left[\frac{N_1}{L}\right] \quad (15)$$

where,

$$N_1 = \frac{(1-\epsilon_{mac})}{\pi R^2} \quad (16)$$

Combination of Eqs. (14) to (16) gives:

$$D_g\frac{dp}{dx^2} - \frac{4D_{le}(1-\epsilon)}{L}\left(\frac{\partial C}{\partial r}\right)_{r=R} = 0 \quad (17)$$

with the following boundary conditions:

$x=0$ $\quad \frac{dp}{dx} = 0$

$x=L$ $\quad p = p_0$

2.4. Ionic overpotential

The overpotential inside the electrode varies in the axial direction. The current density and overpotential relationship are related by Ohm's law, namely:

$$\frac{d\eta}{dx} = \frac{-j(x)}{\pi R^2\kappa_e N_1} \quad (18)$$

where N_1 is given by Eq. (16). The current density generated in a differential axial distance dx is:

$$-dj(x) = 2\pi R N_1 nF D_{le}\left(\frac{dC}{dr}\right)_{r=R}dx \quad (19)$$

Differentiating Eq. (18) gives:

$$\frac{d^2\eta}{dx^2} = -\frac{1}{k_e(1-\epsilon)}\left(\frac{dj(x)}{dx}\right) \quad (20)$$

Substitution of $\frac{dj(x)}{dx}$ from Eq. (19) into Eq. (20) yields:

$$\frac{d^2\eta}{dx^2} = \frac{2nFD_{le}}{k_eR}\left(\frac{dC}{dr}\right)_{r=R} \quad (21)$$

with the following boundary conditions:

$x=0$ $\quad \eta = \eta_0$

$x=L$ $\quad \frac{d\eta}{dx} = 0$

Substituting $\left(\frac{dC}{dr}\right)_{r=R}$ into Eq. (21) produces:

$$\frac{d^2\eta}{dx^2} = \frac{2nFD_{le}C_0}{k_e R}\left[\frac{C_s}{C_0} - \frac{A_3}{A_2}\right] \times\left[\sqrt{\frac{A_1A_2}{C_0}}\coth\left(R\sqrt{\frac{A_1A_2}{C_0}}\right) - \frac{1}{R}\right] \quad (22)$$

To obtain polarization data for the electrode, Eqs. (17) and (22), with their boundary conditions, have to be solved simultaneously. An analytic solution of these equations is not possible. Therefore, a numerical technique is used. In the latter, the given boundary-value problem is converted into an initial-value problem (IVP) by guessing the initial conditions that are not given. Other sets of initial-value problems are generated by differentiating the first set with respect to the assumed values of initial conditions [5]. All these sets are solved simultaneously using the Runge–Kutta method with adjustable step size in double precision.

3. Results and discussion

The developed model was tested in two parts. In the first part, a base set of the parameters was selected by using hydrogen oxidation on Ni/PTFE in 25% KOH electrolyte. Out of these, only one parameter at a time was varied and polarization curves were plotted. The observed effect of that particular parameter was compared with the theoretically expected trend. Individual studies were made of exchange-current density, grain radius, macropore diffusivity, diffusivity in the electrolyte and film thickness. In the second part of the test, the model equations were solved for different temperatures and plotted against experimental polarization data for hydrogen oxidation on Ni/PTFE electrode in 25% KOH electrolyte. The same experimental data were also compared with the previously developed flooded spherical-grain model.

3.1. Effect of parameters on polarization

The prediction of the modified spherical-grain model has been investigated by considering the anodic oxidation of hydrogen in alkaline electrolyte on an Ni/PTFE electrode:

$$H_2(aq) + 2OH^-(aq) \rightleftharpoons 2H_2O(l) + 2e^- \quad (23)$$

The effect of exchange-current density, diffusivity of hydrogen in both macropores and electrolyte, grain size, and film thickness was examined by changing one parameter at a time and fixing the others. For this purpose, the estimated and fitted parameters at 75 °C from Table 1 were selected to test the prediction of the modified model for the performance of a Ni/PTFE electrode in 25% KOH electrolyte. The parameters were as follows:

$\kappa_e = 0.464\ \Omega^{-1}\ cm^{-1}$

$k = 0.507\times10^{-9}$ mol cm^{-3} kPa^{-1}

$D_g = (D'_g)k = 2.279\times10^{-11}$ mol cm^{-1} kPa^{-1} s^{-1}

$D_{le} = 9.529\times10^{-5}\ cm^2\ s^{-1}$

$\delta = 0.8\ \mu m$

$i_0 = 1\ \mu A\ cm^{-2}$

$p_0 = 138$ kPa

The effect of the film thickness (δ) was investigated by varying it in the range from 0.05 to 1 μm. It can be observed from Fig. 2 that, with low values of δ, the current generated for a given overpotential is high due to high diffusion with low film resistance. At higher values of δ and at an overpotential of more than 100 mV, the current density approaches a limiting value. This prediction of limiting current is possible only with the modified model. The previous model fails to show such limiting behavior.

The effect of the exchange-current density (i_0) was studied by varying i_0 from 0.05 to 1.0 $\mu A\ cm^{-2}$, as shown in Fig. 3. It is found that as i_0 increases, the current generated by the electrode increases.

The grain radius (R) affects the polarization performance of the electrode, as shown in Fig. 4 in which R is varied from 15 to 30 μm. The larger the grain radius, the less is the current generated.

The effect of gas diffusivity (D_{le}) in the electrolyte is shown in Fig. 5. D_{le} has been varied from the 5.0×10^{-5} to $20\times10^{-5}\ cm^2\ s^{-1}$. As D_{le} increases, the current density increases for each value of the overpotential. This is expected because more reactant is available for the reaction.

Fig. 6 shows the effect of hydrogen diffusivity (D_g) in the macropores of the electrode for values in the range from 2.5×10^{-12} to 50×10^{-12} mol cm^{-1} kPa^{-1} s^{-1}. As D_g increases, the current density increases. This behaviour reflects the significance of the increase in D_g in higher supply of reactant gas to the electrode.

The reactant pressure profile in the electrode is shown in Fig. 7 for different values of the macropore diffusivity, D_g, in the range from 0.1×10^{-11} to 1000×10^{-11} mol cm^{-1} kPa^{-1} s^{-1}. At higher values of D_g, the pressure in the macropores remains almost constant, since the macropore diffusion resistance is then negligible and the overall reactant is controlled by the electrochemical reaction and/or micropore diffusion. At lower values of D_g, the overall reaction will be macropore-diffusion controlled. At extremely low values, there will be very little reactant available for the reaction, and a limiting current will result.

Table 1
Estimated and fitted parameters for modified model at different temperatures

Temperature (°C)	Estimated parameters from literature				Parameters found from modified model		
	κ (Ω^{-1} cm^{-1})	$k\times10^{9}$ (mol cm^{-3} kPa^{-1})	$D_g\times10^{11}$ (mol cm^{-1} kPa^{-1} s^{-1})	$D_l\times10^{5}$ (cm^2 s^{-1})	α	$\delta\times10^{5}$ (cm)	$i_0\times10^{6}$ (mA cm^{-2})
25	0.254	1.449	4.589	1.515	0.59	7.0	11
35	0.300	1.230	4.097	1.938	0.59	7.0	26
45	0.344	1.0145	3.540	2.625	0.59	7.0	85
55	0.390	0.8696	3.182	3.931	0.59	8.0	160
65	0.434	0.6667	2.551	7.404	0.59	8.0	300
75	0.464	0.5070	2.279	9.529	0.59	8.0	1000

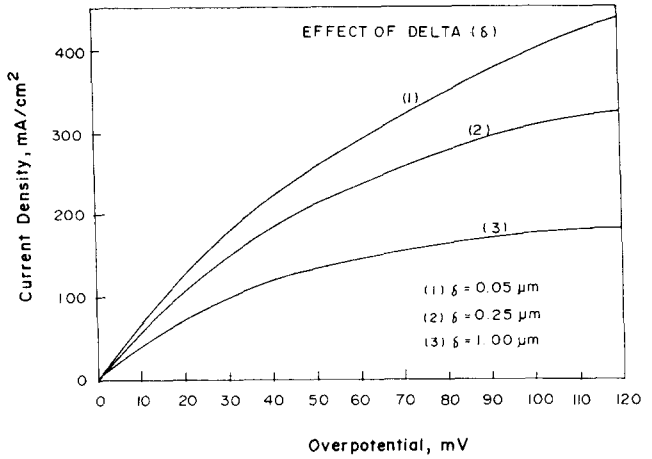

Fig. 2. Effect of film thickness on electrode polarization using parameters at 348 K.

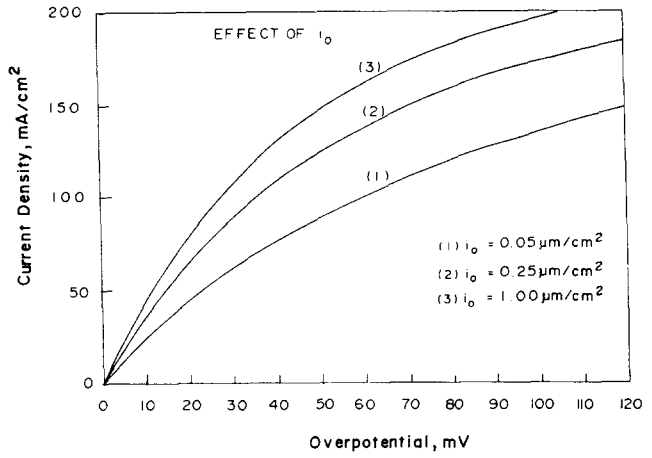

Fig. 3. Effect of exchange-current density on electrode polarization using parameters at 348 K.

3.2. Comparison of modified model prediction with experimentally obtained data

The polarization data for hydrogen oxidation on Ni/PTFE electrodes in 25% KOH electrolyte at different temperatures (25 to 75 °C) has been used for comparison

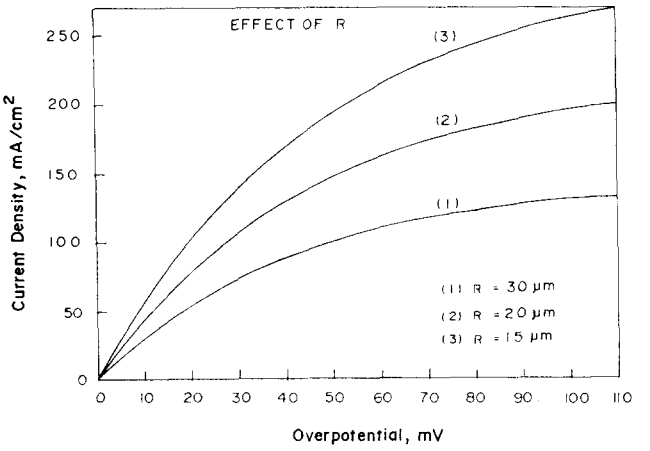

Fig. 4. Effect of grain radius on electrode polarization using parameters at 348 K.

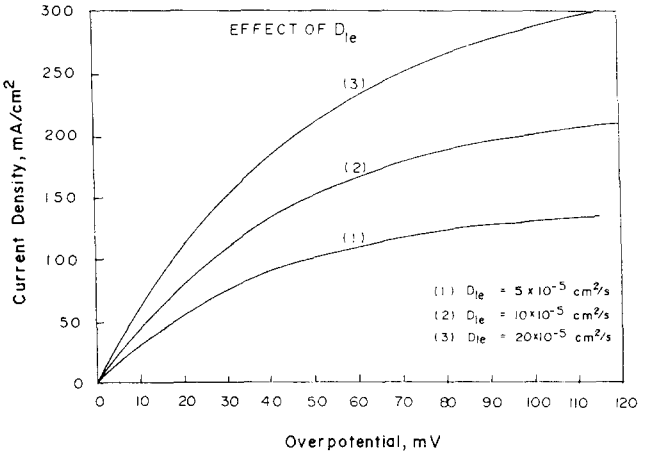

Fig. 5. Effect of diffusivity of hydrogen in electrolyte on electrode polarization using parameters at 348 K.

with data predicted by the modified model. The parameters used to solve the modified model were obtained through electrode characterization, estimation by empirical expressions, and published data. Conductivity of 25% KOH solution was estimated by an empirical formula [6]. The Henry's law constant at different temperatures was obtained from the solubility data

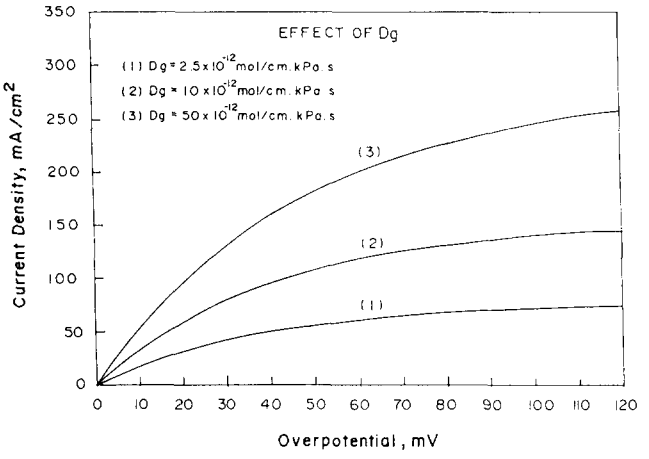

Fig. 6. Effect of diffusivity of hydrogen in macropores on electrode polarization using parameters at 348 K.

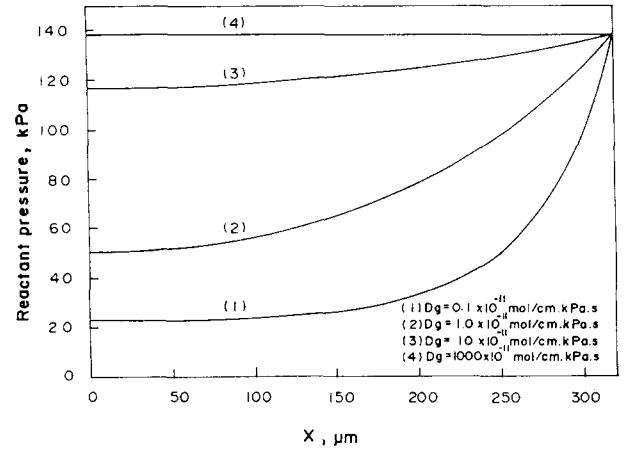

Fig. 7. Reactant pressure profiles in electrode at different macropore diffusivities at $\eta_0 = 44$ mV and other parameters at 348 K.

given by Shoor et al. [7]. The diffusivity of hydrogen in the macropores was calculated by the Hirschfelder's formula [8]. The diffusivity of hydrogen in KOH solution was estimated by a relation given in Ref. [9] using viscosity and density data given in Ref. [10]. With these values, the model equations were solved and fitted to the experimental data (the fitted intrinsic parameters, namely, exchange-current density, charge-transfer coefficient and film thickness, were obtained in this manner). Both estimated and fitted parameters are listed in Table 1. Besides these, the following parameters and constants were also used:

$z = 1.0$

$n = 2.0$

$F = 9.6484531 \times 10^4$ C mol^{-1}

$R = 2.0 \times 10^{-3}$ cm (Ref. [3])

$L = 0.032$ cm (Ref. [3])

$R_g = 8.31$ J mol K^{-1}

$\epsilon_{mac} = 0.21$ (Ref. [3])

$a = 5.4 \times 10^5$ cm^2 cm^{-3} (Ref. [3])

Polarization curves obtained from this modified model, along with the previous model and experimental data are plotted in Figs. 8 and 9 for temperatures of 35, 45, 55 and 75 °C. It is observed that the modified model fits the experimental data very well. It can be inferred from the fitted data that the film thickness remains constant with temperature, while the exchange-current density increases. In fact, the exchange-current density is the electrochemical counterpart of the rate constant for the chemical reactions. Therefore, an Arrhenius' type of temperature dependence is expected. The logarithm of i_0 is plotted against the inverse of the absolute temperature in Fig. 10. The plot is linear and the estimated value of the activation energy is 75.2 kJ mol^{-1}. This value is about twice that predicted by the spherical-grain model [4]. This indicates that the hydrogen oxidation on Ni/PTFE electrode is mass-transfer limited. Since the previous spherical-grain model did not include mass-transfer resistance, the

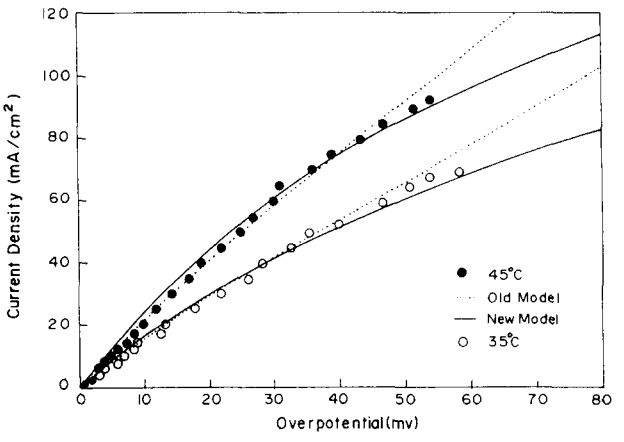

Fig. 8. Comparison of experimental data with old and modified model ($T = 308$ and 318 K).

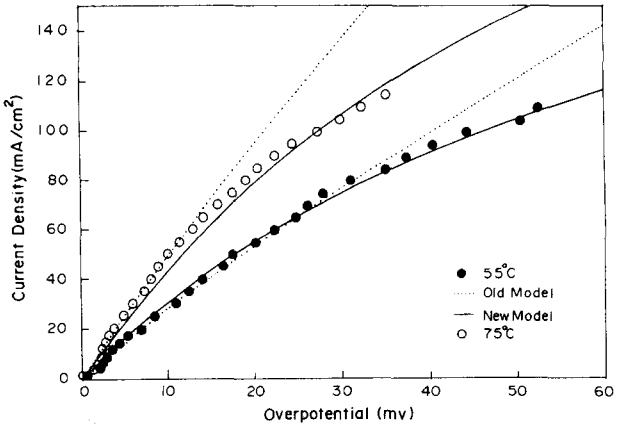

Fig. 9. Comparison of experimental data with old and modified model ($T = 328$ and 348 K).

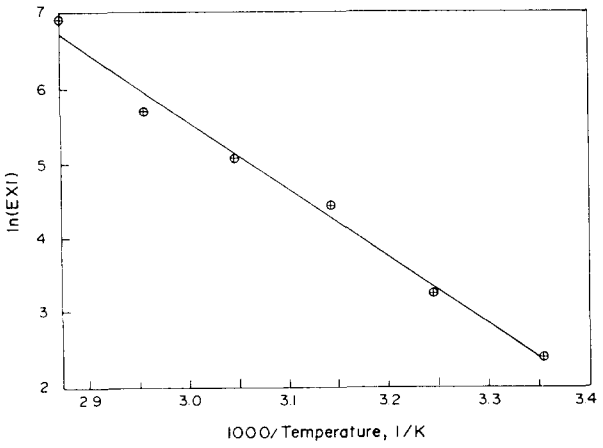

Fig. 10. Exchange-current density vs. 1000/T (Arrhenius' plot).

activation energy calculated was the apparent one. By contrast, the modified model delivers the true value. As expected from mass-transfer-limited catalytic reactions, the apparent activation energy is about half of the true activation energy [11].

4. List of symbols

a surface area of the catalyst (cm^2 per unit volume)
A see Eqs. (5)–(7)
C concentration of reactant in the grain (mol cm^{-3})
C_f concentration of reactant in the film (mol cm^{-3})
C_0 bulk concentration of reactant (mol cm^{-3})
C_S concentration of reactant at the interface of film and grain (mol cm^{-3})
D'_g diffusivity of reactant gas into the macropores (cm^2 s^{-1})
D_g D'_g k (mol cm^{-1} kPa^{-1} s^{-1})
D_l diffusivity of dissolved gas into the electrolyte (cm^2 s^{-1})
D_{le} diffusivity of dissolved gas into flooded grain (cm^2 s^{-1})
F Faraday's constant (9.6484531×10^4 C mol^{-1})
k Henry's constant
i local current density (mA cm^{-2})
i_0 exchange-current density (mA cm^{-2})
j measurable current density (mA cm^{-2})
L thickness of the electrode (cm)
n number of electrons
N_1 number of grains per unit surface area of the electrode (cm^{-2})
p pressure (Pa)
p_0 bulk gas pressure (kPa)
r radial direction (cm)
R grain radius (cm)
R^* consumption of reactant in the electrode (mol cm^{-3} s^{-1})
R_g gas constant (8.314510 J K^{-1} mol^{-1})
r_{gas} consumption of reactants in the grain (mol cm^{-3} s^{-1})
T reaction temperature (K)
x axial direction (cm)
z stoichiometric number

Greek letters

α charge-transfer coefficient
δ film thickness (cm)
η overpotential (mV)
κ_e effective conductivity of the catalyst (Ω^{-1} cm^{-1})
ϵ_{mac} macroporosity of the electrode

Acknowledgements

The authors are grateful to the King Abdulaziz City for Science and Technology (KACST) for financial support under the HYSOLAR project. Thanks are also due to the King Fahd University of Petroleum and Minerals for the use of their facilities.

References

[1] M. Vitanen and J. Lampinen, *J. Power Sources, 32* (1990) 207.
[2] H. Celiker, *Ph.D. Thesis*, King Fahd University of Petroleum and Minerals, Dhahran, Saudi Arabia, 1990.
[3] H. Celiker, M.A. Al-Saleh, S. Gultekin and A.S. Al-Zakri, *J. Electrochem. Soc., 138* (1991) 6.
[4] M.A. Al-Saleh, S. Gultekin, A.S. Al-Zakri and H. Celiker, *Int. J. Hydr. Ener., 19* (1994) 713.
[5] L. Fox, *Numerical Solution of Ordinary and Partial Differential Equations*, Pergamon, Oxford, 1961.
[6] A.L. Horwarth, *Handbook of Aqueous Electrolyte Solutions, Physical Properties, Estimation and Correlations*, Ellis Horwood, Chicester, UK, 1985, p. 252.
[7] S.K. Shoor, R. Duklaker and K.E. Gubbins, *J. Phys. Chem., 175* (1969) 312.
[8] J.O. Hirschfelder, R.B. Bird and E.L. Spotz, *Trans. ASME, 71* (1949) 921.
[9] R.H. Perry and C.H. Chilton, *Chemical Engineers' Handbook*, McGraw Hill, New York, 5th edn., 1982.
[10] V.M.L. Lobo, *Handbook of Electrolyte Solutions – Part A*, Elsevier, Amsterdam, 1989.
[11] J.M. Smith, *Chemical Engineering Kinetics, 3rd ed.*, McGraw-Hill, New York, 1983.